Laboratory and Wind Tunnel Evaluations of the Rosemount Icing Detector

DARREL BAUMGARDNER

Research Aviation Facility, National Center for Atmospheric Research, Boulder, Colorado*

ALFRED RODI

Department of Atmospheric Science, University of Wyoming, Laramie, Wyoming

(Manuscript received 17 June 1988, in final form 17 April 1989)

ABSTRACT

The Rosemount model 871FA ice detector was evaluated during a number of laboratory and wind tunnel studies. The purpose of this evaluation was to determine the sensitivity of the detector to a variety of icing conditions and to determine its utility as a ground-based or airborne liquid water content measuring device.

The laboratory studies determined the ice mass sensitivity of a number of detectors and showed the variability among instruments. These studies also looked at the sensitivity of the detector to the position of mass accumulated on the detector's sensor. The wind tunnel studies determined the dynamic mass response of the detector and demonstrated that this detector can be a very sensitive, fast response, and relatively accurate liquid water content measuring instrument.

1. Introduction

The evolution of hydrometeors in mixed-phase clouds is strongly affected by the amount of supercooled water present at different levels and times during the cloud's development. The formation of graupel and hail is a direct result of the coagulation process by which supercooled water in the form of water droplets is collected by ice crystals as they fall through a cloud. These coagulation processes are not well understood and require more observational studies to unravel their complex mechanisms. The presence of supercooled liquid water is also of great concern in commercial and military aviation because of the effects of airframe icing on aircraft performance. Better measurements are needed to evaluate the macrophysical and microphysical conditions that lead to severe icing events.

There are few instruments which are capable of providing reliable measurements of liquid-water-content (LWC). The most commonly used instruments are hot-wire devices such as the Johnson-Williams (JW) Liquid Water Meter[1] which is described by Neel (1973) and the CSIRO hot-wire probe discussed by King (1978), or light scattering and imaging devices such as those instruments produced by Particle Measuring Systems[2] (Knollenberg 1981). All of these instruments are useful when operated with an understanding of their limitations (Baumgardner 1983); however, none of them give a direct measure of icing rate. Measuring LWCs in mixed phase clouds is particularly difficult because the light scattering and one-dimensional imaging probes cannot distinguish between water and ice. Even the hot-wire probes appear to respond to ice as well as water.

The Rosemount Icing Detector[3] has been used with increasing frequency over the past ten years on both research and commercial aircraft because of the measurement technique with which the rate of ice accumulation is detected. This instrument has negligible sensitivity to ice particles so that it is ideal for applications in mixed phase clouds. This instrument also has the advantage of being less expensive than the instruments previously mentioned; it is extremely easy to mount and operate. In addition, this probe can be operated in ground-based operations with very little support equipment necessary.

The ice probe was designed strictly as an icing rate meter; however, with an understanding of its operating principles and limitations a measure of the LWC may be derived by using additional information typically available on most research and commercial aircraft. Very little has been done to establish the measurement

* The National Center for Atmospheric Research is supported by the National Science Foundation.

[1] Manufactured by Cloud Technology, Palo Alto, California.

[2] PMS, Incorporated, Boulder, Colorado.

[3] Rosemount Engineering, Eden Prairie, Minnesota.

Corresponding author address: Dr. Darrel Baumgardner, Research Aviation Facility. National Center for Atmospheric Research, P.O. Box 3000, Boulder, CO 80307.

limitations of the icing probe and to ascertain its usefulness as a supercooled LWC measuring instrument. The only wind tunnel evaluation of this probe was performed by the manufacturer (Kowles 1973), but the results only indicated its usefulness in measuring icing rate. Musil and Sand (1974) present limited data from flights through thunderstorms and conclude that the results are only accurate for water contents < 1.0 g m^{-3}. Brown (1982) further reinforces this conclusion by presenting additional comparisons of the ice detector with other liquid water content measuring instruments. Most recently, Heymsfield and Miloshevich (1988) compared the icing probe with other liquid water content and particle measuring instruments in an airborne study of cirrus clouds. Their results are useful for providing empirical measures of the icing detector's noise threshold and sensitivity to very low liquid water contents. Lacking in all of these studies is a qualitative assessment of the instrument's mass detecting sensitivity and accuracy as a liquid water content measuring device, with an examination of the physical measuring principles and evaluation of its performance under carefully controlled conditions. The lack of such information was the motivation for the present study.

The Rosemount probe was tested during a series of laboratory studies to establish accurate mass-to-voltage calibrations and to determine the sensitivity of this calibration to the position of accumulated mass on the sensor. In addition, sensors of the same model were tested to establish the variability of operating characteristics from probe to probe.

Wind tunnel studies were conducted in an icing wind tunnel in order to compare the actual and predicted response of the probe and to determine the conditions under which the icing probe might be used as an instrument for measuring supercooled LWC.

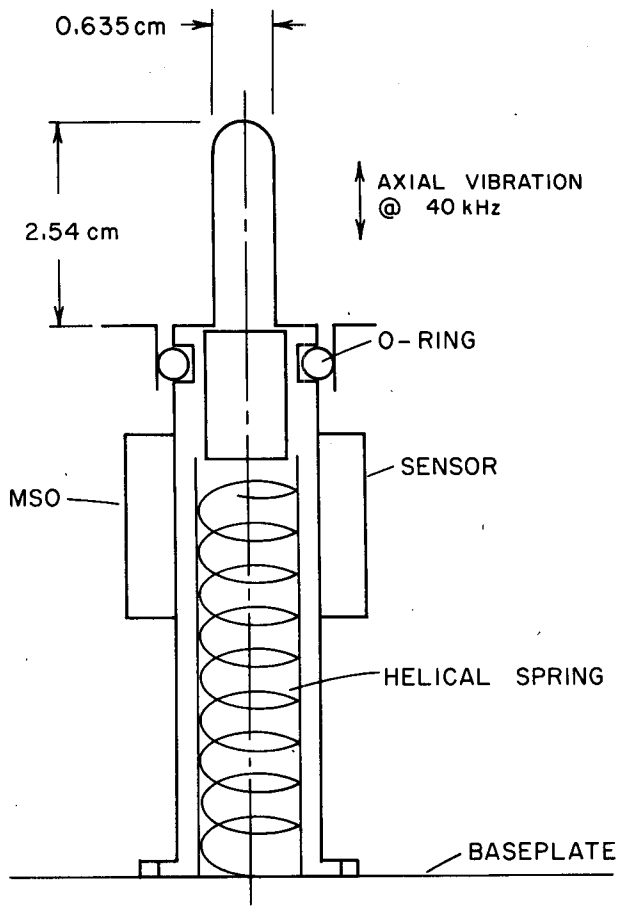

FIG. 1. This schematic is a conceptual representation of the magnetostrictive oscillator (MSO), the principal component of the icing probe. The O-ring forms the node about which the sensor oscillates symmetrically.

2. Theory of operation

The exposed element of the ice detector is a 0.635 cm diameter, nickel alloy cylinder that is excited electrically to vibrate longitudinally at a natural frequency of 40 kHz. The decrease in frequency that results from ice accumulating on the probe is sensed and converted to a voltage, which is recorded. Hill and Woffinden (1980) examined theoretically the response of a vibrating wire of 0.6 mm diameter for collecting ice at an airflow rate of 5 m s^{-1} in a special balloon-launched radiosonde. In order to examine the relationship between mass and frequency of the Rosemount probe sensing element, a simple model of the probe geometry is used to predict the frequency change. The sensing element is considered to be a hollow cylinder, mounted rigidly and allowed to vibrate longitudinally at its principal mode (Fig. 1), the nodal position being the O-ring which is 2.54 cm from the top. Classical mechanics predicts the natural frequency to be

$$\omega_1 = \frac{\pi}{2}\left(\frac{EA}{ml^2}\right)^{1/2} = \frac{\pi}{2}\left(\frac{E}{\rho l^2}\right)^{1/2} \quad (1)$$

where

A cross-sectional area of the cylinder (assumed hollow with inner and outer diameters of 4.35 $\times 10^{-3}$ and 6.35 $\times 10^{-3}$ m, respectively),
l length [.0254 m],
E modulus of elasticity,
m mass per unit length, ($=\rho \star A$),
ρ density of the material,
ω angular frequency.

Since the natural frequency (nominally 40 kHz) and geometry of the probe are known, we can estimate the value of the modulus of elasticity by solving (1) for E. The estimated value is approximately 135 GPa, which is reasonable for this material.

Two modes of mass accretion are modeled: (1) adding mass at the tip of the sensing element, and (2) adding mass uniformly along the length of the cylinder. For the small masses added to the tip, the natural frequency can be calculated from the expression

$$\omega_1 = \frac{\pi}{2}\left[\frac{EA}{\rho A l^2 + 2M_0 l}\right]^{1/2} \quad (2)$$

where M_0 is the mass added. For masses added uniformly along the length of the cylinder, the frequencies can be calculated from the expression

$$\omega_1 = \frac{\pi}{2}\left[\frac{E}{(\rho + (m_0/Al))l^2}\right]^{1/2}. \quad (3)$$

The resulting changes from the zero-mass frequency is plotted in Fig. 2. In these calculations, we have shown the effect of changing the density of the material (and thus its value of E) in order to demonstrate the uncertainty caused by not knowing the exact properties of the material.

The mass added to the tip has a larger effect on frequency than those distributed evenly along the length. This can be explained by the larger inertial effect of the mass concentrated at the tip where the amplitude of the vibration is the largest.

These calculations predict that the frequency changes expected for 50–80 mg added to the probe (masses which "trip" the probe as described below) to be 500–900 Hz for the mass concentrated on the tip. While these calculations are intended to be a rough indication of probe sensitivity, they demonstrate that probe frequency is expected to be linear (for these small masses added) and dependent on the location of the deposition.

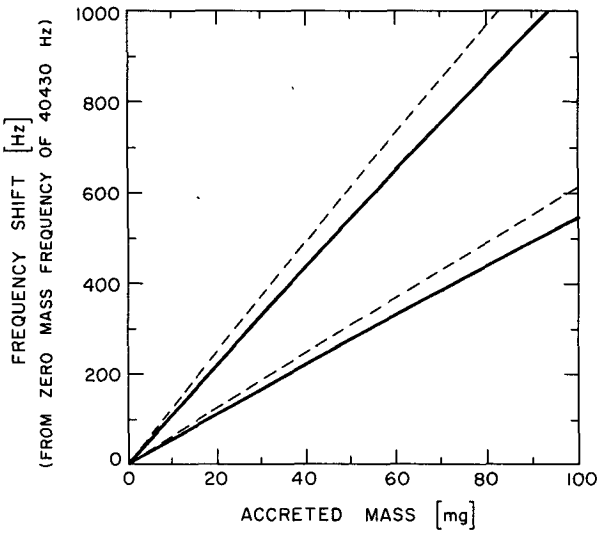

FIG. 2. The calculated frequency shift is shown here as a function of the accreted mass. The upper solid line is for mass on the tip of the sensor; the lower solid line is for mass evenly distributed along the sensor. The dashed lines are similar to the solid lines except for a different assumed value of the sensor material density and modulus of elasticity. (ρ = 8500 Kg m^{-3}, E = 143 GPa for the solid line; ρ = 7500 Kg m^{-3}, E = 126 GPa for the dashed line).

The frequency is compared to the specified reference frequency of about 40.2 kHz, converted to a voltage and output as a frequency of 200 Hz with zero ice present (operating manual). The probe "trips," i.e., de-ices, when the frequency difference increases to 350 Hz for nominally 0.05 cm ice accumulation (Kowles 1973). When the mass is distributed evenly along the length of the probe, our simple model predicts the probe to deice at about 30 mg accumulation (150 Hz frequency shift in Fig. 2). We test these statements of nominal probe operation in section 3.

3. Laboratory evaluation

The precision with which this icing sensor responds to mass accretion was investigated in the laboratory. The method used was to place carefully measured drops of water onto the sensing element after it had been cooled in a freezer. Other variations of this method involve the use of paint (Hill and Woffinden 1980) and transparent tape (Brown 1982). The former investigators have suggested that the properties of the applied (accreted) mass are not important to the vibration changes of the element provided that the mass is relatively small. The ice mass method was selected in this study because of the small increments that can be added (on the order of 1 mg/drop), as well as for the fact that the calibration is done at temperatures likely to be encountered in actual research operations. Further, with this method, the ice could be deposited at various locations on the sensing element in order to demonstrate the sensitivity discussed in section 2.

Droplets are formed with a hypodermic syringe where the droplet mass depends upon the rate at which the plunger on the syringe advances. The plunger is advanced by a digitally controlled precision stepping motor attached to a micrometer screw. The drop mass is measured by weighing 10 or more drops on a microbalance and corrections are applied for the evaporation rate of the sample. Twenty drops were weighed over a ten minute period and the average evaporation rate was measured at 3.15% per minute at room temperature and at 0.8% per minute at −10°C. This evaporation rate was thought to be negligible within the accuracy of the experiment and no corrections were applied to the measurements. The error in weighing the drops on the microbalance was estimated to be 0.5 mg for a sample of 20 mg.

One problem with this technique is the difficulty caused by the surface tension when removing the drop from the tip of the syringe. The surface tension is overcome by touching the drop to the surface to which it is deposited; variations can occur in drop mass at given drop gun settings because of this. Care was taken within

each set of tests to minimize this variation. A second difficulty resulted from the use of water at room temperature in the syringe since time was required for the drops to freeze on the subcooled sensing element. This time could be shortened by the use of a chilled needle to nucleate each drop after deposition. The drop masses used in the tests and reported here were typically 1–2 mg.

The variation of sensing element vibration frequency to mass accumulation is shown in these tests to be very sensitive to the location of the ice as explained in the discussion of probe operation. The vibrational frequency was very sensitive to mass deposited at the sensing element tip and very insensitive to mass at the base. In Fig. 3, the output voltage versus mass is plotted for mass deposited at the sensing element tip, midway along the element, and evenly along the length, respectively. The "trip" point is seen to be 21 mg for mass at the tip, 36 mg for mass at the middle, and 37 mg for mass evenly deposited. The application of the mass uniformly along the element is considered to be most representative of the natural icing of the probe on the aircraft.

It was determined that the "trip" point varies widely from sensor to sensor when a number of probes were tested. In Table 1, the trip points of four sensors are listed for a series of tests where the mass was distributed evenly along the length of the sensor. These results suggest that frequent calibration of these probes is mandatory for the data to be useful in a quantitative sense. It should be noted that some of the variation among individual probes resulted from the fact that the trip point is optionally set to be 0.5 mm or 1.0 mm thickness of ice (nominally) according to the specifications of the user.

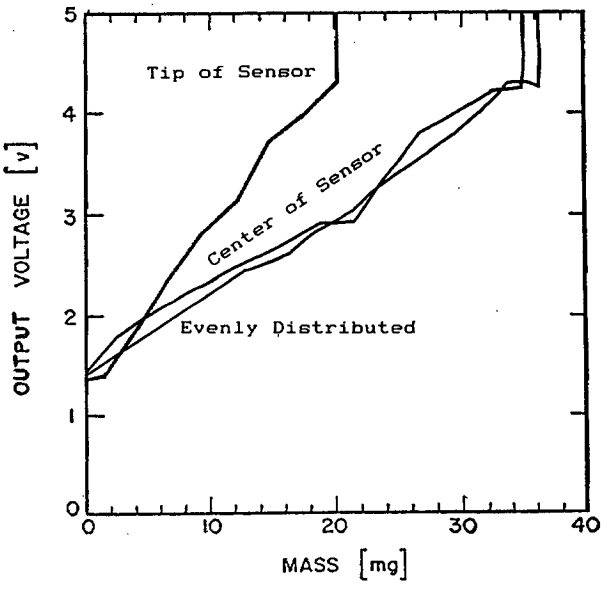

FIG. 3. The output voltage is shown here as a function of the accreted mass for several different accretion locations on the icing probe. The upper curve is for mass at the tip; the middle curve is for mass in the middle; and the lower curve is for mass distributed evenly along the sensor.

TABLE 1. Mass and output voltage at trip point for various icing rate probes.

Serial	Mass (mg)			Voltage (V)	Temp (°C)
288	75.6			4.52	−15
	75.6			4.38	
	75.6	average	75.6	4.51	
096	133.5			5.08	−15
	156.2	average	144.8	5.12	
484	25.6			4.84	−13
	23.1			5.08	
	25.6	average	26.2	4.46	
	30.4	SD	2.655	4.42	
495	19.5			4.17	−18
	15.8			4.76	
	17.1			4.90	
	17.1			5.14	
	14.6			4.85	
	19.0			4.98	−15
	41.2	average	22.0	4.93	
	31.7	SD	8.807	4.98	

The laboratory evaluations allow an estimate of the sensitivity of the ice probe to very small liquid water contents. At the minimum drop mass of 1.0 mg used in these studies, the voltage output of the probe was well above the zero mass level. For an aircraft flying 100 m s^{-1} the ice probe would accrete this much ice over a 100 m path length for a LWC of approximately 0.05 g m^{-3}; LWCs on the order of 0.01 g m^{-3} or less should be easily detectable over path lengths > 500 m. The results of Heymsfield and Miloshevich (1988), who determined a threshold of 0.002 g m^{-3} from observational data, reinforce this conclusion.

4. Wind tunnel evaluation

a. Tunnel characteristics and operating procedure

In April of 1981 and again in April of 1983, wind tunnel studies were conducted for the purpose of calibrating, evaluating, and comparing a number of various instruments used for the airborne measurement of LWC. These tests were carried out at the Low Temperature Laboratory of the National Research Council of Canada with the cooperation and guidance of the Atmospheric Environment Service of Canada.

The wind tunnel used for these studies is a high speed, closed circuit icing tunnel capable of producing Mach 0.9 in the 30 cm × 30 cm × 45 cm test section. Temperatures may be controlled to as low as −40°C with an accuracy of ±0.5°C. The LWC can be provided

to greater than 3 g m^{-3}, depending upon the airspeed. The median volume diameter of the spray droplets range from 10 μm to 30 μm, depending upon the LWC. Additional details concerning the operating characteristics and calibration of this tunnel are described by Strapp and Schemenaur (1982).

The LWC distribution across the test section was mapped using a JW to measure the relative changes as it was moved from one side to the other of the tunnel. The LWC profile from this measurement is shown in Fig. 4. Since the JW is sensitive to airspeed as well as LWC changes, the velocity profile was determined with a Pitot tube. This measurement is also shown on Fig. 4 where it may be seen that the changes measured by the JW are only a result of decreasing LWC value rather than decreasing velocity. The ice probe's position relative to the LWC distribution is also seen on Fig. 4, showing that the sensor intercepted approximately 60–80% of the nominal LWC during an icing test.

The ice probe (same serial number probe both years) was mounted along with a JW probe in the tunnel and the analog data from both instruments sampled and digitized at a 1 Hz rate and recorded for subsequent analysis. Figure 5 shows the relative positions of both instruments. The icing tests were conducted over a variety of conditions as tabulated in Table 2, and each condition was maintained for a period of 30 seconds.

b. Wind tunnel results

Figure 6 illustrates the typical response of the ice probe after the onset of an icing condition. There are several observations to be made from this figure. At 15/28/00 the water is off but the ice probe still retains ice from a previous test run where the water was turned off before the ice detector's trip point was reached. This condition is evidenced by the constant output voltage of 2.4 V. When the water is turned on at 15/28/29 the voltage increases as the mass accumulates until the preset trip point of 4.5 V is reached at 15/28/43. At this point the heater is turned on automatically for a period of ≈5 s and the output voltage returns to its zero mass value. Although the water is still on during this period, as shown in Fig. 6, the output voltage is sporadic for a period of about 14 s before a more uniform rate of voltage increase occurs. This behavior results since a period of time is required for the sensor to cool after the heat cycle before reaching the freezing temperature again. This period of time is governed by the convective and conductive heat transfer characteristics between the probe, adjoining support and air. When possible, this delay period was measured for each test condition (see Table 3). The results are somewhat

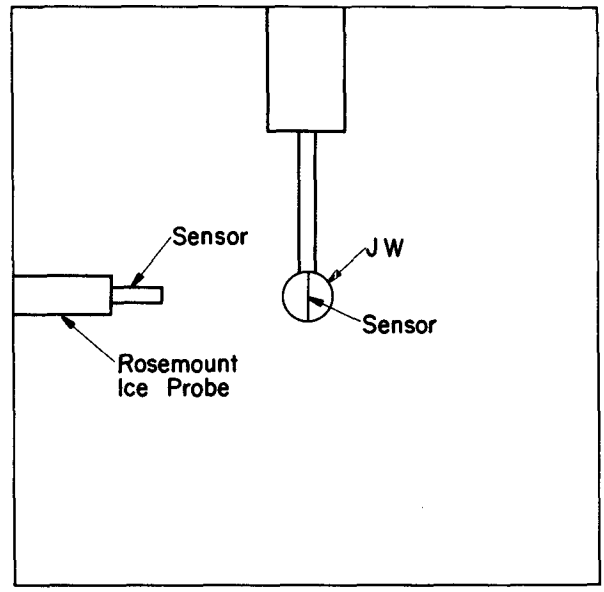

FIG. 5. A schematic cross section of the wind tunnel is shown here illustrating the relative positions of the ice probe and JW liquid water probe.

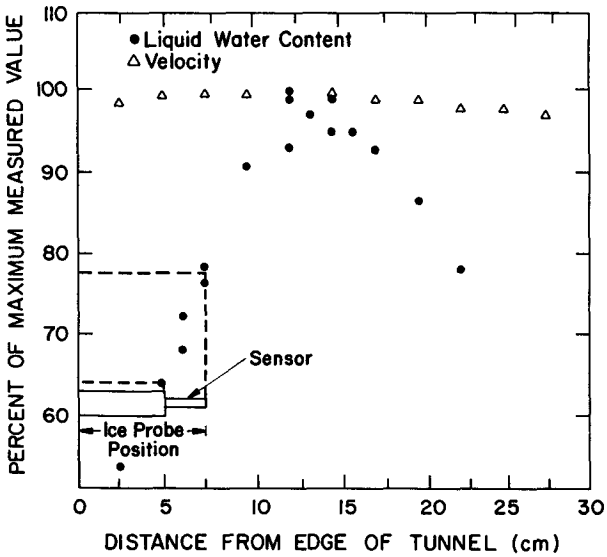

FIG. 4. The liquid water and velocity profiles as a function of distance from the wind tunnel wall are shown in this diagram. The sensor outline shows the distance that it extended from the wall of the tunnel.

TABLE 2. Wind tunnel test conditions.

Airspeed ($m\ s^{-1}$)	Temperature (°C)	Liquid water contents ($g\ m^{-3}$)
77	−20	0.1, 0.2, 0.4, 0.6, 0.8, 1.0, 1.2, 1.4, 1.6, 1.8, 2.0
77	−10	0.1, 0.2, 0.4, 0.6, 0.8, 1.0, 1.2, 1.4, 1.6, 1.8, 2.0
103	−10	0.2, 0.6, 1.0, 1.4, 1.6, 2.0
103	−5	0.2, 0.6, 1.0, 1.4, 1.6, 2.0
77	−5	0.2, 0.4, 0.6, 0.8, 1.2, 1.5, 1.7, 1.9, 2.1, 2.3, 2.7

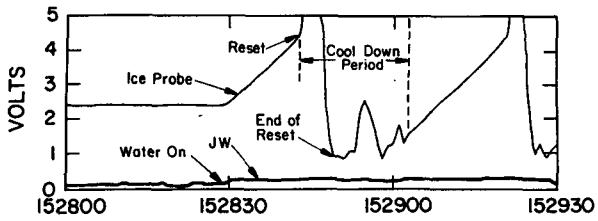

FIG. 6. The output response of the ice probe and JW is shown as a function of time.

surprising since the delay times would be expected to decrease with decreasing temperature and increasing airspeed rather than the opposite, as observed.

Once the voltage-to-mass calibration has been determined as discussed in section 3, a relationship may be found between the voltage rate of change (dV/dt) and the LWC. The mass accumulated on the sensor is just

$$M = E_c \cdot d \cdot l \cdot v \cdot W \cdot t \tag{4}$$

where

E_c collection efficiency of the sensor
d diameter of the sensor
v airspeed
W liquid water content
t accumulation time.

Thus the mass accumulation rate is

$$w = \left[\frac{1}{E_c \cdot d \cdot l}\right] \frac{dM}{dt} \Big/ v \tag{5}$$

and if the voltage-to-mass calibration is

$$V = GM \tag{6}$$

where G is the gain factor and

$$\frac{dV}{dt} = G \frac{dM}{dt} \tag{7}$$

then

$$\frac{dV}{dt} = G \cdot E_c \cdot d \cdot l \cdot v \cdot W. \tag{8}$$

Figures 7 and 8 show the average measured dV/dt as a function of the LWC. The dV/dts are measured as the voltage difference between consecutive one second data points. During each temperature and water condition, the dV/dts are averaged and standard deviations about the average are computed. These are shown as bars in the ordinate direction at each data point. The bars drawn in the abscissa direction indicate the range of LWCs that arise from the LWC distribution shown in Fig. 4.

The dV/dt increases linearly with increasing LWC until, in some cases such as shown in Fig. 7, an apparent plateau is reached, above which increases in LWC produce no increases in the dV/dt. This plateau is probably a result of reaching the Ludlam limit (Ludlam 1951); i.e., the critical cloud water content where droplets are shed from the accreting ice surface when the surface temperature rises above the melting point because of latent heat release and adiabatic compression of the air stream at the ice surface. This temperature increase also causes a diffusion of water vapor from the ice surface because of the difference in vapor pressures between the ice surface and surrounding air. This theoretical water content is plotted in Fig. 9 as a function of airspeed for the three temperatures used in the wind tunnel tests. The calculations incorporate the geometry of the ice probe and environmental conditions that were present during the tests. Also plotted on the same figure are the estimates of the LWC where apparent shedding was occurring during the icing runs. These estimates are derived from Figs. 7 and 8 by examining the point where the dV/dt versus LWC trend appears to become nonlinear. The bars on the graph reflect the uncertainty of this measurement technique for such a small number of data points where a precise inflection point is impossible to determine. Visual ob-

TABLE 3. Summary of wind tunnel results.

		Airspeed = 77 m s^{-1}		Airspeed = 103 m s^{-1}	
	−20°C	−10°C	−5°	−10°C	−5°C
Predicted slope MV m^3 s^{-1} g^{-1}	501	501	501	670	670
Actual slope MV m^3 s^{-1} g^{-1}	n = 13 334	n = 10 364	n = 4 323	n = 5 495	n = 6 408
Normalized slope V m^2 g^{-1}	65.7 ± 6.9	69.6 ± 6.8	62.6 ± 7.6	73.7 ± 12.3	62.5 ± 7.8
Cool off delay period (seconds)	n = 4 23.8 ± 1.7	n = 10 16.8 ± 1.8	n = 8 13.3 ± 0.7	n = 1 15	n = 9 15.9 ± 1.5

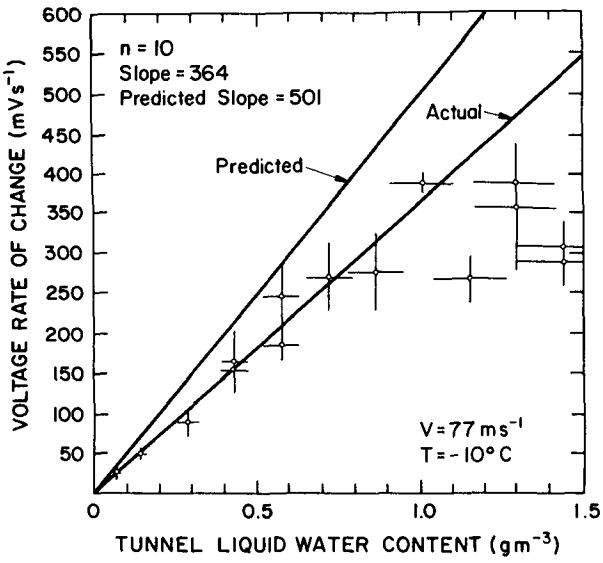

FIG. 7. The voltage rate of change as a function of liquid water content during the wind tunnel tests is shown for a tunnel velocity of 77 m s^{-1} and a temperature of −10°C.

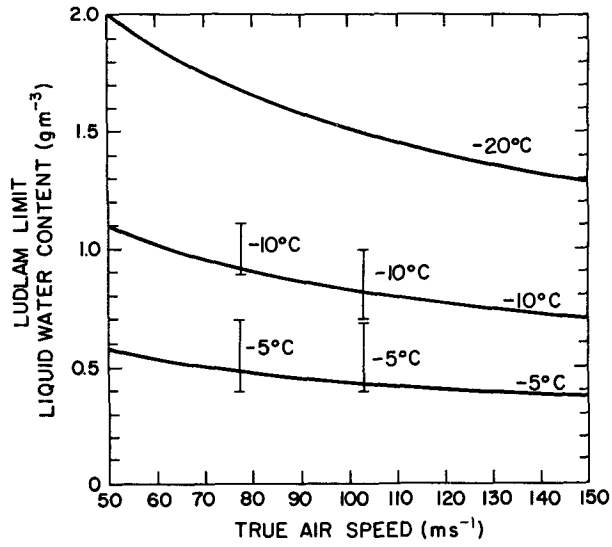

FIG. 9. The Ludlam limit is shown as a function of the airspeed for several temperature regimes. The bars represent estimates of the measured Ludlum limit from the wind tunnel tests.

servations during the tests could not detect actual shedding until the LWC was well beyond the Ludlum limit. The comparison between actual and theoretical in Fig. 9 suggests that the measured values are within a factor of 2 of the predicted.

There are two linear curves drawn on Figs. 7 and 8 which represent the predicted and actual dV/dt-to-LWC relationships. The predicted slope (with the effect of airspeed taken out) is derived from (8) as

$$\text{Predicted slope} = G \cdot E \cdot d \cdot l \qquad (9)$$

where the gain, G, was established from the laboratory calibration as 67.2 V g^{-1} and E is approximately 0.55 for v = 77 m s^{-1}, and 0.6 for v = 103 m s^{-1}. These values were calculated using the experimental results of Ranz and Wong (1952) for a cylindrical body and assuming a droplet diameter of 17 μm, a temperature of −10°C, and a static pressure of 1020 mb. The difference between the actual and predicted slopes suggests that an error was made in the assumption(s) used in deriving the predicted slope. The actual and predicted slopes tabulated in Table 3 show similar results as those seen in Figs. 7 and 8. These results lead to two observations. First, the predicted slope should increase by a factor of 1.33 for a change in airspeed from 77 to 103 m s^{-1}. The observed change is approximately by this factor which indicates that the difference between the predicted and actual slopes is probably not a function of airspeed. Second, the ratio of predicted to actual slopes is approximately the same for all conditions.

An examination of (9) shows that uncertainties in the gain, collection efficiency, sensor diameter and length determine the accuracy of estimating the slope of the relation between dV/dt and LWC. There is an uncertainty in determining the diameter of the probe since this dimension increases with mass accumulation—a trend which should cause the slope to increase rather than decrease, as observed. The maximum expected increase in diameter is estimated by assuming that the maximum mass accumulation of approximately 60 mg builds up with a density of 0.8 g m^{-3} on the front half of the sensor. This produces an increase of approximately 2 mm, or about +30%.

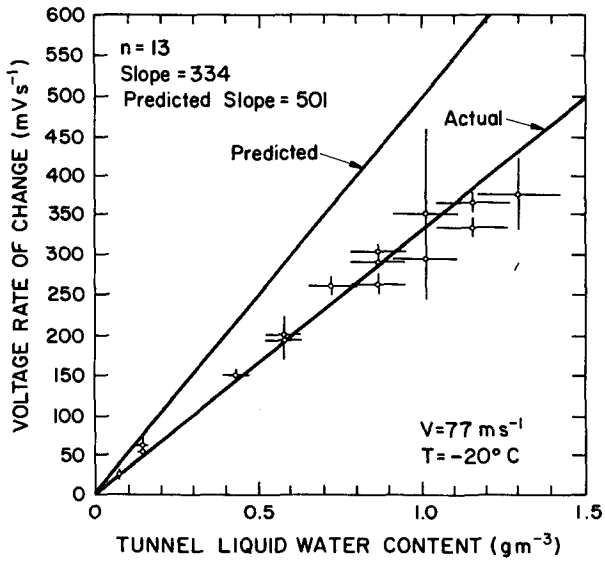

FIG. 8. As in Fig. 7 except for a temperature of −20°C.

As discussed in sections 2 and 3, the voltage-to-mass sensitivity of the ice detector is strongly dependent upon where the mass accumulates on the sensor. Since the location of ice on the sensor will be affected by the liquid water distribution across the cross section of the tunnel, the position sensitivity of the sensor is probably a significant contributor to the slope differences. The observations showed that the sensor accreted ice nonuniformly along its length; however, it was impossible to establish exactly where the center of mass of the ice was located. Thus the gain, which is position dependent, is uncertain to $\approx \pm 30\%$.

The assumed collection efficiency is based upon the median volume diameter of droplets which implies that 50% of the water mass is contained in droplets less than that diameter. There remains an uncertainty of approximately ±20% in the collection efficiency values used in the evaluation of (9) which accounts for a large portion of the observed differences in slopes.

Finally, the entire length of the sensor is used in (9); however, it is unlikely that the portion of the sensor closest to the support intercepts many, if any, of the droplets due to the airflow around the support which shadows a portion of the sensor. A rough estimate based on the observed ice accumulation indicates that approximately 10% of the sensor would be shadowed by this effect.

The uncertainty in the evaluation of the predicted slope can be estimated using the propagation of errors and neglecting the effects of any correlations among the errors. This estimate takes the form

$$e_{slp}^2 = e_G^2 + e_E^2 + e_d^2 + e_l^2 \qquad (10)$$

where e_x is the estimated standard deviation of the quantity x, which in this case is G, E, d, and l.

On substitution of the estimated values for the error in G, E, d, and l, the total estimated error in predicted slope is +48%, −37%. This admittedly rough approximation indicates that the actual slope values are not unreasonable in light of the possible errors in assumed values used for evaluating (9). Thus, if (9) is used to derive LWC values from dV/dt measurements, with no other calibration data available, the subsequent LWC would be accurate to at least ±48%.

The LWC is calculated from the dV/dt as

$$\mathrm{LWC} = \frac{1}{G \cdot E \cdot d \cdot l \cdot v} \cdot \frac{dV}{dt}. \qquad (11)$$

The normalized slope, defined as the ratio of the predicted slope to airspeed, was also derived from the wind tunnel data as a function of the airspeed, LWC, and measured dV/dt (see Table 3). Only those data points were used where the slope was linear and there were no signs that the Ludlum limit had been exceeded. If the slope is computed over all conditions, and the uncertainty in intercepted LWC is taken into account, the average slope is 67.6 V m^2 g^{-1} ±8.3. When this value is used in (11) to determine LWC, the accuracy in LWC is < ±20%, a significant improvement in accuracy over using theoretical predictions of LWC.

Heymsfield and Miloshevich (1988) derived a slope of 15.6 V m^2 g^{-1} from airborne intercomparisons, which is significantly smaller than found in this study. However, there can be a wide difference in G, the mass to voltage relation. The values found in this study (Table 1) ranged from 35.5–226 V m^2 g^{-1}. Since the gain is not known for the probe in the study by Heymsfield and Miloshevich, their results can not be compared directly with those of this study.

5. Conclusions

Comparisons of the theoretically predicted response of the Rosemount ice probe with laboratory and wind tunnel measurements confirm that this instrument has a relatively well-behaved, linear, response to supercooled liquid water as long as shedding does not take place as a result of exceeding the characteristic Ludlum limit for the probe. The liquid water content can be derived from the accretion rate measurement to an accuracy of approximately 50% if only the theoretical response equation is used. However, laboratory and wind tunnel calibrations can increase this accuracy to nearly 20% by obtaining empirical values for the gain factor for a particular probe and by reducing the uncertainty in sample area.

The ice probe is extremely sensitive to very small liquid water contents and is theoretically limited only by the path length needed to accrete at least a milligram of ice on its sensor.

The primary limitation of this instrument is the sensitivity of its response to the location at which ice accretes on the sensor. Since laboratory calibrations cannot account for the accretion geometry, which is possibly a function of the airflow distortion caused by the probe and the mounting location, airborne measurements would be helpful in establishing the response sensitivity of a probe in a given mounting location.

Finally, all four instruments studied in the laboratory were found to have different mass sensitivity. This result indicates that each instrument must be characterized individually in order to obtain accurate measurements of liquid water content.

Acknowledgments. The work done at the University of Wyoming was supported by the Bureau of Reclamation, Division of Atmospheric Resources Research, under Contract 2-07-81-v0256. Glen Gordon, Ken Waight, and Filipe Serrano helped with the laboratory experiments. We gratefully thank Dr. Andrew Hanson at the University of Wyoming, Department of Mechanical Engineering, for helpful discussions on the

theory of probe operation, and Ms. Karen Bowie, of the Research Aviation Facility-NCAR, for preparation of this manuscript.

REFERENCES

Baumgardner, D., 1983: An analysis and comparison of five water droplet measuring instruments. *J. Appl. Meteor.*, **22,** 891–910.

Brown, E. N., 1982: Ice detector evaluation for aircraft hazard warning and undercooled water content measurements. *J. Aircraft,* **19,** 980–983.

Heymsfield, A. J., and L. M. Miloshevich, 1988: Evaluation of liquid water measuring instruments in cold clouds sampled during FIRE. *J. Atmos. Oceanic Technol.,*.

Hill, G. E., and D. S. Woffinden, 1980: A balloonborne instrument for the measurement of vertical profiles of supercooled liquid water concentration, *J. Appl. Meteor.*, **19,** 1285–1292.

Knollenberg, R. G., 1981: *Techniques for Probing Cloud Microstructure: Clouds, Their Formation, Optical Properties, and Effects.* P. V. Hobbs and A. Deepak, Eds., Academic Press, 495 pp.

Kowles, J., 1973: A discussion of icing rate measurement and the Rosemount icing rate system. Rosemount Rep. 67312A, 18 pp.

Ludlam, F. H., 1951: The heat economy of a rimed cylinder, *Quart. J. Roy. Meteor. Soc.*, **77,** 663–666.

Musil, D. J., and W. R. Sand, 1974: Use of the Rosemount icing rate probe in thunderstorm penetrations. *Atmospheric Technology, Winter 1974–1975,* National Center for Atmospheric Research, Boulder, Co., 140–142.

Ranz, W. E., and J. B. Wong, 1952: Impaction of dust and smoke particles. *Ind. Eng. Chem.*, **44,** 1371–1381.

Strapp, J. W., and R. S. Schemenaur, 1982: Calibrations of Johnson–Williams liquid water content meters in a high speed icing tunnel. *J. Appl. Meteor.*, **21,** 98–108.